Simulation of TaO_X-RRAM with Ta_2O_{5-X}/TaO_{2-X} Stack Engineering

Y.D. Zhao, P. Huang, Z. Chen, C. Liu, H.T. Li, W.J. Ma, B. Gao, X.Y. Liu, J.F. Kang
Institute of Microelectronics
Peking University
Beijing, China
kangjf@pku.edu.cn

***Abstract*—An atomistic Monte-Carlo simulator of TaO_X-based resistive random access memory (RRAM) with bi-layered Ta_2O_{5-X}/TaO_{2-X} stack is developed by considering generation/recombination (G-R) of oxygen vacancies (V_O) with oxygen ions (O^{2-}), phase transition (P-T) between Ta_2O_5 and TaO_2 as well as interactions of Ta_2O_{5-X}/TaO_{2-X} stack. The stack induced effects involving changeable Schottky barrier (SB) at the stack interface, the evolutions of O^{2-} and lattice oxygen (LO) in the stack and the self-compliance effect are also included in the simulator. Using the simulation tool, the resistive switching (RS) characteristics of the bi-layered TaO_X-based RRAM can be reproduced. The impacts of different stack thicknesses, oxygen contents and capabilities to take redox reactions with O^{2-} of TaO_{2-X} layer on RS behaviors are simulated. The simulation results can be utilized to achieve controllable switching processes and optimized device performances.**

Keywords*—RRAM, resistive switching, conductive filament, TaO_X, Monte-Carlo, simulation.

I. Introduction

TaO_X-based resistive random access memory (RRAM) has encouraged extensive study recently due to its fast switching speed, compatibility with CMOS technology and superior endurance property [1-10]. The resistive switching (RS) characteristics of TaO_X-based RRAM are complicated due to the asymmetric bi-layered device structure and the multiple Ta-O compositions. Understanding the key factors correlated with RS behaviors of TaO_X-based RRAM devices is imperatively needed for device optimization and future applications.

In this work, an atomistic Monte-Carlo simulator of bi-layered TaO_X-based RRAM is developed taking account of the impacts of generation/recombination (G-R) of oxygen vacancies (V_O) with oxygen ions (O^{2-}) and phase transition (P-T) [11] between Ta_2O_5 and TaO_2 on RS behaviors. In addition, the interactions of Ta_2O_{5-X}/TaO_{2-X} stack are included in the simulator which involve changeable Schottky barrier (SB) at the stack interface, the evolutions of O^{2-} and lattice oxygen (LO) in the stack as well as the stack induced self-compliance effect. Using the developed simulation tool, the impacts of different thicknesses, oxygen contents and capabilities to take redox reactions with O^{2-} of TaO_{2-X} layer can be simulated to achieve controllable switching processes and optimized properties.

II. Simulation Methods

A typical structure of TaO_X-based RRAM consists of a Ta_2O_{5-X} resistive switching layer (RSL) and an oxygen deficient TaO_{2-X} base layer (TBL) as shown in Fig. 1(a) [5,6]. TBL acts as a self-compliance layer and an oxygen reservoir. As illustrated in Fig. 1(b), during SET process, the stoichiometric Ta_2O_5 can be transformed to two possible conductive structure phases: V_O-defected Ta_2O_5 or TaO_2. When the conductive filament (CF) consisting of V_O-defected Ta_2O_5 and TaO_2 connects top electrode and conductive TBL, the device is switched to low resistance state (LRS) and SB effect between RSL and TBL is eliminated. When CF is ruptured during RESET and the device is in high resistance state (HRS), SB between semiconductor-like RSL and conductive TBL should be considered.

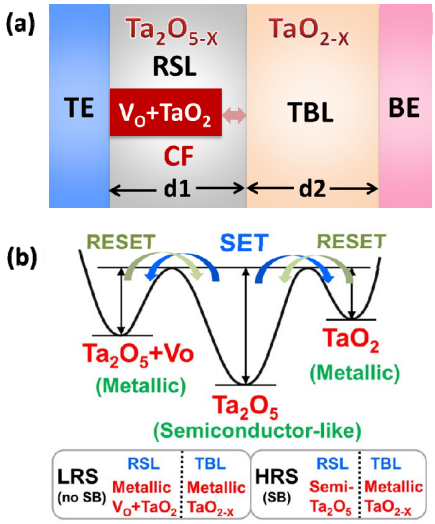

Fig. 1 (a) Device structure of bi-layered TaO_X-based RRAM composed of a Ta_2O_{5-X} resistive swithing layer (RSL) and TaO_{2-X} base layer (TBL). d1 and d2 are thicknesses of RSL and TBL respectively. (b) Energy levels of Ta_2O_5, V_O-defected Ta_2O_5 and TaO_2. The Schottky barrier (SB) exists between RSL and TBL at high resistance state (HRS).

978-1-4673-7860-4/15/$31.00 ©2015 IEEE

The RS dynamics include: 1) G-R of V_O with O^{2-} under applied bias; 2) P-T between Ta_2O_5 and TaO_2 under thermal effect; 3) O^{2-} migration from RSL towards TBL during SET and reversely during RESET; 4) redox reactions in TBL including O^{2-} stored as LO and O^{2-} release by TBL decomposition assisted by heat; 5) current rectified with changeable SB height due to Fermi-level pinning effect at the interface of Ta_2O_{5-X}/TaO_{2-X} stack.

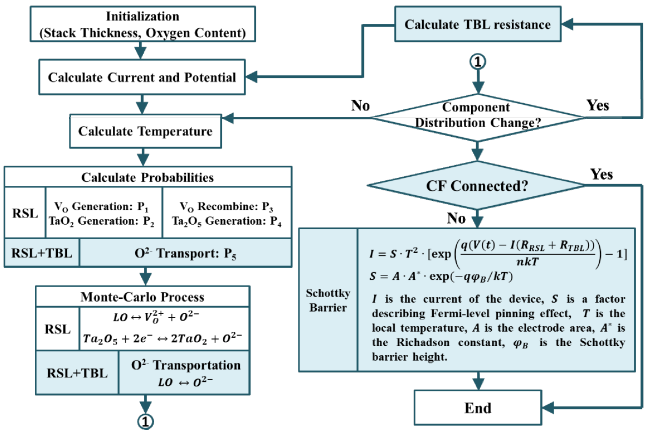

Fig. 2 Simulation flow chart of the simulator. Colored parts are related with the interactions of Ta_2O_{5-X}/TaO_{2-X} stack.

An atomistic Monte-Carlo simulator is developed to quantify above processes. Fig. 2 is the simulation flow chart. In order to clearly show the impacts of Ta_2O_{5-X}/TaO_{2-X} stack on RS behaviors, the related simulation processes are marked with colors in Fig. 2. Based on the XPS depth analysis of the bi-layered stack, the thicknesses of Ta_2O_{5-X}/TaO_{2-X} stack and the distributions of Ta_2O_{5-X} and TaO_{2-X} with different oxygen contents can be extracted as the inputs of the simulation. After that, the potential and current distributions in TaO_X-based RRAM are solved by the resistance network in the simulator, and then the local temperature is calculated. Following these, the probabilities of G-R, P-T, and the transportation of O^{2-} during SET and RESET processes are calculated respectively. By using Monte-Carlo methods, the processes of G-R, P-T, transportation of O^{2-} and transition between LO and O^{2-} can be decided. After one above process takes place, the resistance of TBL should be recalculated because the change of LO contributes to the change of resistance in TBL. If the CF is not connected between top electrode and TBL, the SB should be considered and the current is rectified with changeable SB height during different operation conditions. The above calculation processes will be repeated as the sweeping voltage changes.

III. Results and Discussions

The electrical characteristics and microscopic behaviors of bi-layered TaO_X-based RRAM can be simulated by the developed Monte-Carlo simulator. TaO_X-based RRAM with 20nm Ta_2O_{5-X}/20nm TaO_{2-X} stack is simulated and the simulation results are compared with the measured data on the fabricated devices with $Pt/Ta_2O_{5-X}/TaO_{2-X}/Ta$ structure. Electrical measurements were performed with Agilent-33250A pulse generator and Agilent-B1500 analyzer. By considering SB effect, the measured multi-level I-V characteristics can be reproduced by the simulator as shown in Fig. 3. The multi-level characteristics are realized by applying different RESET stop voltages, which are 1.3V, 1.8V and 2.3V respectively. Excellent agreements are achieved between measurements and simulations by considering different SB heights in these cases. In order to figure out the impacts of G-R and P-T on RS behaviors of bi-layered TaO_X-based RRAM, the I-V characteristics considering G-R, P-T and both effects are simulated and compared with measurements as shown in Fig. 4. Results reveal that SET/RESET voltages correlated with P-T are much higher than that with G-R and RS is due to combined effects of G-R and P-T while G-R dominates RS.

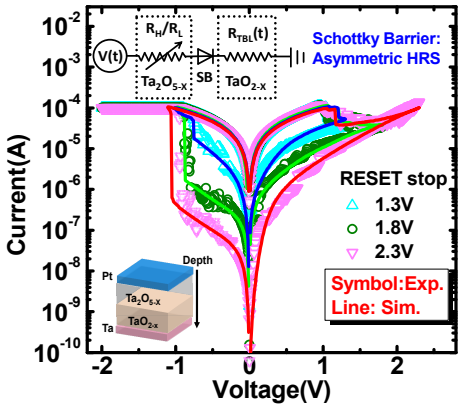

Fig. 3 Measured and simulated multi-level I-V curves of TaO_X-based RRAM using different RESET stop voltages. Taking Schottky barrier into consideration, excellent agreements are got between measurements and simulations. Inset is the equivalent circuit of the device.

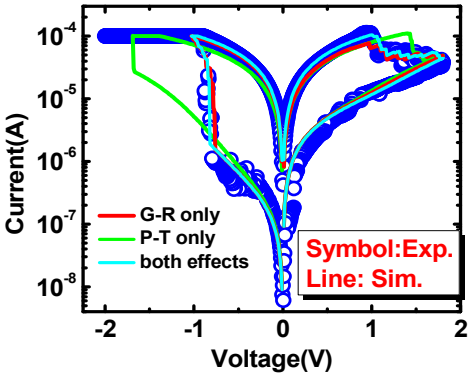

Fig. 4 Simulated I-V curves considering G-R, P-T and both effects as RS mechanism and their comparisons with measurements. The I-V characteristics considering both G-R and P-T effects best agrees with measurements.

Fig. 5 is the simulated microscopic evolution of CF and distributions of both dissociative O^{2-} and stored LO during switching with 20nm Ta_2O_{5-X}/20nm TaO_{2-X} stack. As shown in Fig. 5(a), during SET process, CF composed of V_O and TaO_2 connects top electrode and TBL. The generated O^{2-} drift into TBL under electric field and are absorbed by TaO_{2-X} as LO. During RESET process as shown in Fig. 5(b), O^{2-} and LO in TBL are activated to RSL to rupture CF at the interface of RSL

and TBL. The proportion of TaO_2 in CF can be predicted by simulations in Fig. 6. Fig. 6(a) shows that the increase of compliance current (CC) during Forming under same ambient temperature (Ta) will result in the increase of TaO_2 ratio in CF. Fig. 6(b) demonstrates that the increase of Ta under same CC during Forming will lead to the increase of TaO_2 proportion in CF.

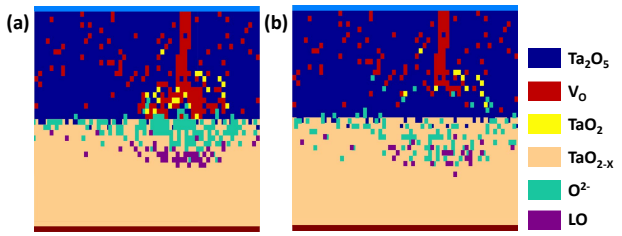

Fig. 5 Simulated microscopic evolutions of CF and distributions of both dissociative O^{2-} and stored lattice oxygen (LO) after (a) SET and (b) RESET processes of device with 20nm Ta_2O_{5-X}/20nm TaO_{2-X} stack. CF is composed of V_O and TaO_2. The generated O^{2-} drifted into TBL can be absorbed by TaO_{2-X} as LO.

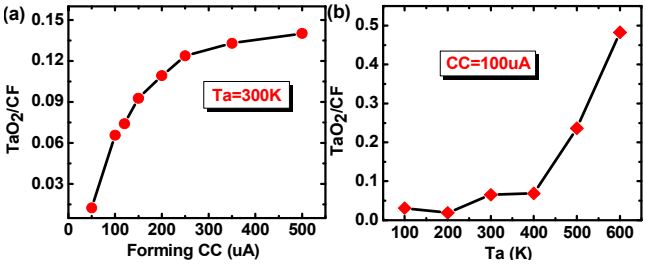

Fig. 6 (a) The increasing ratio of TaO_2 in CF with increasing compliance current (CC) during Forming under same ambient temperature (Ta). (b) The increasing ratio of TaO_2 in CF with increasing Ta under same CC during Forming.

In order to explore the impacts of different TBL on RS behaviors, devices with different TBL thicknesses and oxygen contents are simulated. Bi-layered TaO_X-based RRAM devices with different TBL thicknesses are shown in Fig. 7. Fig. 7(a)-(c) are simulated CF and oxygen distributions of devices with 20nm/10nm, 20nm/20nm and 20nm/40nm Ta_2O_{5-X}/TaO_{2-X} stacks respectively. Fig. 7(d) shows corresponding SET characteristics with same CC. Results reveal that TBL with the thickness close to RSL are beneficial for self-compliance. The large V_{SET} induced high local temperature of 40nm TBL results in wide CF which accounts for the relatively large current during SET.

Ta_2O_{5-X}/TaO_{2-X} stacks with different oxygen contents in TBL are simulated in Fig. 8. Fig. 8(a)-(c) are CF after FORMING and corresponding current profile under 2V applied voltage with O/Ta ratio of 1/2, 1 and 2, respectively. The higher oxygen content corresponds to higher TBL resistance [7]. Simulated SET characteristics of cases (a)-(c) are shown in Fig. 8(d). Results indicate that devices with higher oxygen content of TBL have better self-compliance characteristics. However, high oxygen content of TBL also results in relatively large SET voltage. Stack thickness and oxygen content tradeoffs are needed to balance SET voltage, SET speed, self-compliance and power characteristics.

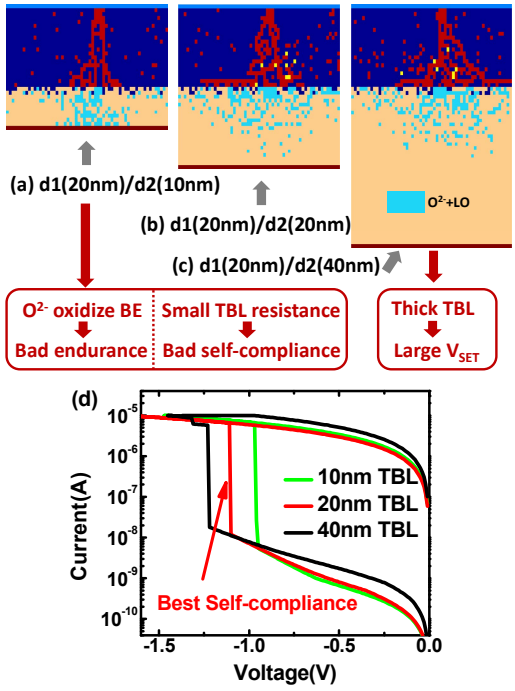

Fig. 7 (a-c) CF and oxygen distribution after FORMING in Ta_2O_{5-X}/TaO_{2-X} stack with different TaO_{2-X} thicknesses. (d) Simulated SET characteristics of cases (a)-(c).

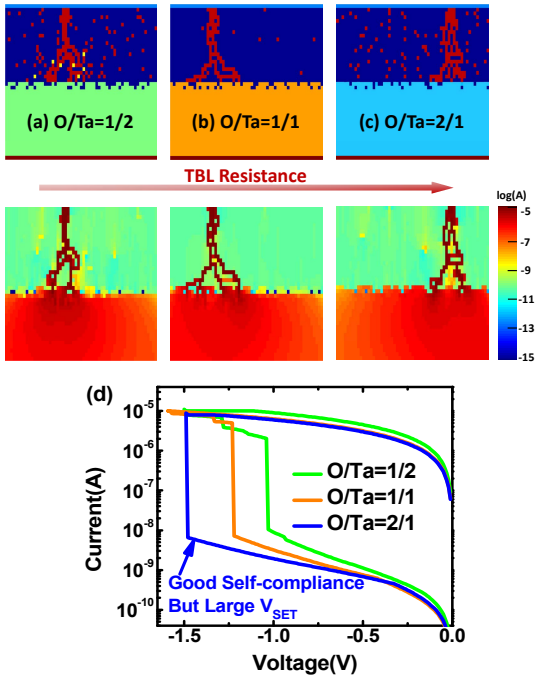

Fig. 8 (a-c) CF after FORMING and corresponding current profile (applied voltage: 2V) in Ta_2O_{5-X}/TaO_{2-X} stack with different oxygen contents in TBL. The higher oxygen content corresponds to higher TBL resistance. (d) Simulated SET characteristics of cases (a)-(c).

O^{2-} and LO distributions in TBL are determined by the capability of TBL to take redox reactions with O^{2-} as shown in Fig. 9. TBL in Fig. 9(a) is difficult to take redox reactions with O^{2-} and thus the dissociative O^{2-} can hardly be stored as LO in TBL. O^{2-} will disperse in TBL under electric filed and thermal effects, leading to the dispersive oxygen distribution in TBL. This will result in the degradation of HRS after several cycles when the left O^{2-} near CF region is insufficient to rupture CF. Fig. 9(b) shows the case when TBL can easily take redox reactions with O^{2-}. In this case, TBL can easily store O^{2-} as LO during SET and decompose to release O^{2-} assisted by heat during RESET. The oxygen distribution in Fig. 9(b) is more concentrated than in Fig. 9(a), assuring the supply of O^{2-} during RESET to rupture CF.

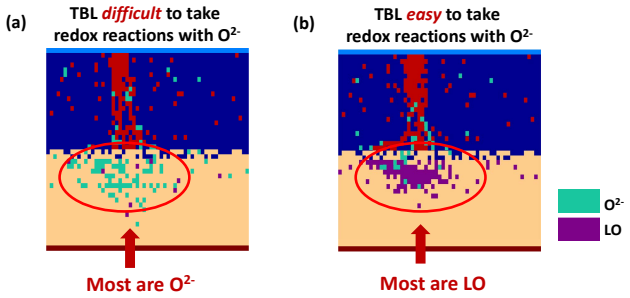

Fig. 9 Distributions of O^{2-} and LO after SET when TBL is (a) difficult or (b) easy to take redox reactions with O^{2-}.

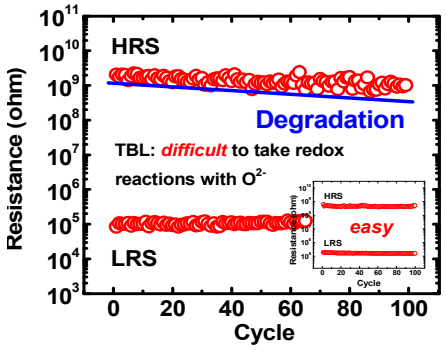

Fig. 10 Endurance degradation of 100 cycles when TBL is difficult to take redox reactions with O^{2-}. Inset is the case of TBL easy to take redox reactions. HRS/LRS represent high/low resistance state.

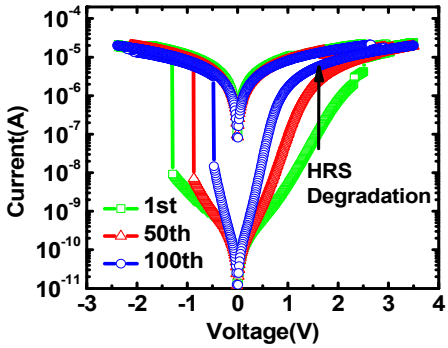

Fig. 11 Degradation of resistance window of the 1st, 50th and 100th cycles when TBL is difficult to take redox reactions with O^{2-}.

Fig. 10 shows the simulated endurance degradation of 100 cycles when TBL is set to be extremely difficult to take redox reactions with O^{2-}. Inset in Fig. 10 is the case when TBL is easy to take redox reactions with O^{2-} and no obvious degradation of HRS is observed. Fig. 11 shows the I-V characteristics of the 1st, 50th and 100th cycles in the degraded case of Fig. 10. The resistance window is gradually reduced during 100 switching cycles, revealing the degradation of HRS.

IV. Conclusion

An atomistic Monte-Carlo simulator is developed to simulate the RS behaviors of bi-layered TaO_X-based RRAM. Excellent agreements between simulation results and experimental data are achieved. The developed simulator can be used to predict the optimized thickness and oxygen content of Ta_2O_{5-X}/TaO_{2-X} stack for future device optimization design such as enhanced RRAM reliability.

Acknowledgment

The authors would like to thank Ji Ding, Jonathan England and Hasan Nejad at Applied Materials, Rob Elliman and Dinesh Venkatachalam at Australian National University. This work is partly supported by 973 Program (2011CBA00600) and NSFC Program (61421005/61334007).

References

[1] H.-S. P. Wong, H.-Y. Lee, S. Yu, *et al.* , "Metal-Oxide RRAM," *Proc. IEEE*, vol. 100, no. 6, pp. 1951-1970, June 2012.

[2] R. Waser and M. Anono, "Nanoionics-based resistive switching memories," *Nat. Mater.*, vol. 6, pp. 833-840, Nov. 2007.

[3] J. J. Yang, D. B. Strukov, and D. R. Stewart, "Memristive devices for computing," *Nat. Nanotech.*, vol. 8, no. 13, pp. 13-24, Dec. 2012.

[4] T. -Y. Liu, T. H. Yan, R. Scheuerlein, *et al.*, "A 130.7mm^2 2-Layer 32 Gb ReRAM Memory Device in 24 nm Technology," in *IEEE ISSCC Dig. Tech. Papers*, pp. 210-211, 2013.

[5] Myoung-Jae Lee, Chang Bum Lee, Dongsoo Lee, et al., "A fast, high-endurance and scalable non-volatile memory device made from asymmetric Ta_2O_{5-X}/TaO_{2-X} bilayer structures," *Nat. Mater.*, vol. 10, pp. 625-630, Aug. 2011.

[6] Young-Bae Kim, Seung Ryul Lee, Dongsoo Lee, et al., "Bi-layered RRAM with Unlimited Endurance and Extremely Uniform Switching," in *Proc. IEEE Symp. VLSI Technol.*, Jun. 2011, pp. 52-53.

[7] Z. Wei, Y. Kanzawa, K. Arita, et al., "Highly Reliable TaO_X ReRAM and Direct Evidence of Redox Reaction Mechanism," in *Proc. IEEE IEDM*, Dec. 2008, pp. 1-4.

[8] L.Goux, A. Fantini, A. Redolfi, et al., "Role of the Ta scavenger electrode in the excellent switching control and reliability of a scalable low-current operated TiN\Ta_2O_5\Ta RRAM device," in *Proc. IEEE Symp. VLSI Technol.*, Jun. 2014, pp. 162-163.

[9] Chung-Wei Hsu, Chia-Chen Wan, I-Ting Wang, *et al.*, "3D Vertical TaO_X/TiO_2 RRAM with over 10^3 Self-Rectifying Ratio and Sub-μA Operating Current," in *Proc. IEEE IEDM*, Dec. 2013, pp. 264-267.

[10] Ken Kawai, Akifumi Kawahara, Ryutaro Yasuhara, *et al.*, "Highly-reliable TaOx ReRAM Technology using Automatic Forming Circuit," in *IEEE ICICDT*, May. 2014, pp. 1-4.

[11] Y. D. Zhao, P. Huang, Z. Chen, et al., "Insights into Resistive Switching Characteristics of TaO_X-RRAM by Monte-Carlo Simulation," in *Proc. VLSI-TSA*, 2015, pp. 1-2.